The Astrophysical Journal, 714:1120–1132, 2010 May 10 doi:10.1088/0004-637X/714/2/1120


# ROTATIONAL SPECTRUM AND TENTATIVE DETECTION OF $DCOOCH_3$–METHYL FORMATE IN ORION

L. Margulès[1], T. R. Huet[1], J. Demaison[1], M. Carvajal[2], I. Kleiner[3], H. Møllendal[4], B. Tercero[5], N. Marcelino[5], and J. Cernicharo[5]

[1] Laboratoire de Physique des Lasers, Atomes, et Molécules, UMR CNRS 8523, Université Lille 1, F-59655 Villeneuve d'Ascq Cédex, France; laurent.margules@univ-lille1.fr

[2] Departamento de Física Aplicada, Facultad de Ciencias Experimentales, Universidad de Huelva, 21071 Huelva, Spain

[3] Laboratoire Interuniversitaire des Systèmes Atmosphériques, UMR CNRS 7583, Université Paris 7 et Université Paris 12, 61 av. Charles de Gaulle, F-94010 Créteil Cédex, France

[4] Centre for Theoretical and Computational Chemistry (CTCC), Department of Chemistry, University of Oslo, P.O. Box 1033 Blindern, NO-0315 Oslo, Norway

[5] Centro de Astrobiología (CSIC-INTA), Laboratory of Molecular Astrophysics, Department of Astrophysics, Ctra de Ajalvir, Km 4, 28850 Torrejón de Ardoz, Madrid, Spain; jcernicharo@cab.inta-csic.es

*Received 2009 June 19; accepted 2010 March 5; published 2010 April 16*

## ABSTRACT

New centimeter-wave (7–80 GHz) and submillimeter-wave (580–661 GHz) spectra of a deuterated species of methyl formate ($DCOOCH_3$) have been measured. Transitions with a maximum value of $J = 64$ and $K = 36$ have been assigned and fitted together with previous measurements. The internal rotation of this compound was treated using the so-called rho axis method. A total of 1703 transitions were fitted using this method. Only 24 parameters were employed in the final fit, which has an rms deviation of 94.2 kHz. The dipole moment and the nuclear quadrupole coupling constants of the deuterated specie have also been obtained. This new study has permitted a tentative detection of $DCOOCH_3$ in Orion with the IRAM 30 m telescope based on the observation of more than 100 spectral features with low blending effects among the 400 lines expected in the observed frequency domain (for which over 300 are heavily blended with other species). These 100 transitions are above noise and confusion limited without heavy blending and cannot be assigned to any other species. Moreover, none of the strongest unblended transitions is missing. The derived source-averaged total column density for $DCOOCH_3$ is $7.8 \times 10^{14}$ cm$^{-2}$ and the $DCOOCH_3/HCOOCH_3$ column density ratio varies between 0.02 and 0.06 in the different cloud components of Orion. This value is consistent with the deuteration enhancement found for other species in this cloud.

*Key words:* ISM: molecules – line: identification – methods: data analysis – methods: laboratory – methods: observational – submillimeter: ISM

*Online-only material:* color figures, machine-readable table

## 1. INTRODUCTION

Methyl formate ($HCOOCH_3$) has been detected in the hot cores of giant molecular clouds such as Orion KL, Sgr B2(N), and W51 e1/e2, in star-forming regions, and in comets (Blake et al. 1986; Nummelin et al. 2000; Lovas 2004; Kobayashi et al. 2007; Demyk et al. 2008). The relatively large abundance of methyl formate in hot core sources has led to the identification of an important number of interstellar lines. Approximately 900 lines of the ground torsional state were detected in various interstellar molecular clouds, Sgr B2, Orion KL, and W51 e1/e2 (Lovas 2004). Recently, torsionally excited lines of methyl formate were also observed in Orion KL by Kobayashi et al. (2007) and in W51 e2 by Demyk et al. (2008). The $^{13}C$ species of methyl formate were also subject of astrophysical searches, and about 400 lines belonging to $HCOO^{13}CH_3$ and $H^{13}COOCH_3$ were very recently detected (Carvajal et al. 2009).

Despite the fact that methyl formate is such an abundant ubiquitous interstellar molecule and that isotopic fractionation effects involving deuterium are prevalent in the interstellar medium (Herbst 1992), the singly deuterated isotopologues of methyl formate have not been detected yet. As already pointed out by Oesterling et al. (1995), the absence of detection is weird because deuterated isotopologues of methanol ($CH_3OD$ and $CH_2DOH$) have been detected in the interstellar medium (Mauersberger et al. 1988; Jacq et al. 1993). We should emphasize that the identification of interstellar normal methyl formate and its $^{13}C$ isotopologues was only made possible thanks to comprehensive laboratory work. The large spectral material, which is now available for methyl formate, is required to make full use for the new radio-astronomy facilities (*Herschel*, ALMA, SOFIA). The reason of this comprehensive experimental and theoretical work is due to the fact that the structure of the methyl formate spectrum is complicated by the combination of a large amplitude motion, the torsion, with the large asymmetry splittings occurring in this fairly asymmetric near-prolate rotor ($\kappa = -0.75$ for $DCOOCH_3$). In particular, the internal rotation of the methyl group splits each rotational line into a doublet (characterized by the symmetry labels A and E). As the molecule is light and as the barrier to internal rotation is not so high, the internal rotation splittings are relatively large and the transition frequencies are thus difficult to calculate with accuracy, especially at high $J$ values, without appropriate theory. The singly deuterated methyl formate isotopologue $DCOOCH_3$ was not studied as much as the normal species or even the $^{13}C$ species (Willaert et al. 2006; Carvajal et al. 2007, 2009; Maeda et al. 2008a, 2008b; Ilyushin et al. 2009), or the mono-deuterated methyl formate $HCOOCH_2D$, which was also recently investigated (Margulès et al. 2009a) at high resolution. Curl (1959) has studied different isotopic species of methyl formate, measuring the microwave spectrum of $DCOOCH_3$ up to 30 GHz, identifying 27 rotational transitions, and analyzing the internal rotation splittings and spectra using the principal axis method (PAM). He also determined the components of the electric dipole moment along the $a$ and $b$ principal axes. Oesterling et al. (1995) extended the measurements of the spectra to a frequency of

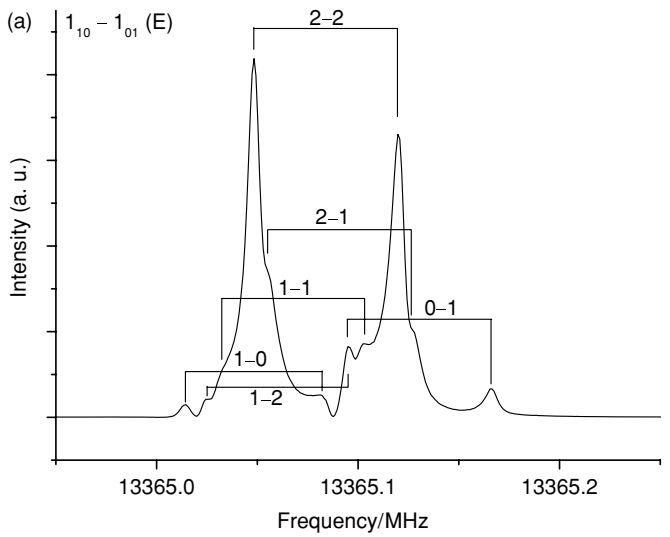


**Figure 1.** $1_{10}$–$1_{01}$ (E) transition with hyperfine components due to nuclear spin of deuterium, recorded with the FTMW spectrometer.

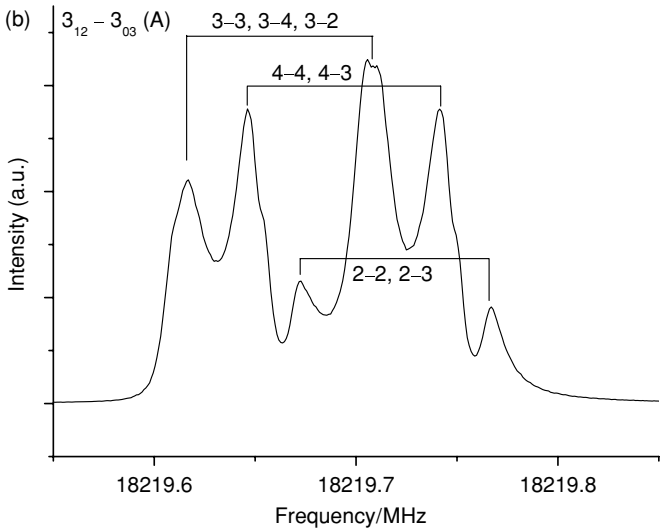


**Figure 2.** $3_{12}$–$3_{03}$ (A) transition with hyperfine components due to nuclear spin of deuterium, recorded with the FTMW spectrometer.

377 GHz and assigned lines up to $J = 30$. These authors then combined their 885 new lines with the 27 lines from Curl's measurement using a global internal axis method, and obtained an rms deviation of 85 kHz with 31 parameters.

In the present paper, we continue our review of methyl formate isotopologues, trying to compile all previously published microwave and submillimeter data, and completing the measurements in certain spectral ranges. Using the so-called rho axis method (RAM), we have studied the normal species (Carvajal et al. 2007), the H$^{13}$COOCH$_3$ and HCOO$^{13}$CH$_3$ (Willaert et al. 2006; Carvajal et al. 2009) isotopologues. It should be noted that, using the same RAM approach, the microwave spectrum of the normal species of methyl formate was reinvestigated by Ilyushin et al. (2009) who incorporated all previously published measurements, including the measurements from Maeda et al. (2008a, 2008b) as well as 1550 remeasurements and 1769 new measurements from Kharkov in the 49–150 GHz frequency range, improving substantially the fit with a unitless weighted rms deviation of 0.71 for 10,533 lines (6952 $v_t = 0$ and 3581 $v_t = 1$) and reaching the experimental uncertainty for both $v_t = 0$ and 1 torsional states. The impressive analysis performed by Ilyushin et al. (2009) using the same RAM approach shows the success of this method despite the internal rotors with intermediate barrier height, and high $J$ and $K$ values are dealt with (up to $J = 64$, $K_a = 36$ in the ground $v_t$ torsional state and up to $J = 35$, $K_a = 23$ in the first excited torsional state $v_t = 1$). Following the analysis we have performed for the $^{13}$C isotopologues in our previous paper (Carvajal et al. 2009), we have searched for this species in the 30 m IRAM line survey of Orion (Tercero et al. 2010). Although the lines are weaker, and many of them blended with other species, we found evidences for a tentative detection of deuterated methyl formate based on more than 100 spectral features.

## 2. EXPERIMENTS

### *2.1. Lille: FTMW spectrometer*

The hyperfine structure of DCOOCH$_3$ was observed using the new molecular beam Fourier transform microwave (FTMW) spectrometer of Lille. The basic principles and technical details remain unchanged (Kassi et al. 2000). The main improvement of the new spectrometer consists of two new mirrors (diameter of 0.7 m compared to 0.4 m previously), in order to improve the signal-to-noise ratio at low frequencies (diffraction losses). Signals were recorded in the 4–18 GHz spectral region. Methyl formate vapors at a pressure of 20 mbar were mixed with neon carrier gas at a backing pressure of 1.5 bar. The mixture was introduced into a Fabry–Perot cavity at a repetition rate of 1.5 Hz. Molecules were polarized within the supersonic expansion by a 2 $\mu$s pulse and the free induction decay signal was detected and digitized at a repetition rate of 120 MHz. After transformation in the time domain signal, molecular lines were observed as Doppler doublets, with a signal point at every 0.92 kHz, resulting from the average of about 100 co-added signals. Transition frequency was measured as an average of the two Doppler components, and for most of the lines the uncertainty of the measurements is estimated to be less than 2 kHz. A typical example of signals, associated with the $1_{10}$–$1_{01}$ (E) and $3_{12}$–$3_{03}$ (A) rotational transitions, is displayed (Figures 1 and 2). The quadrupole hyperfine structure associated with the D atom is clearly observed. In the case of the A components, weak additional features are observed in some lines. They are most probably due to the spin–spin interaction between the two equivalent hydrogen atoms and were not further considered.

### *2.2. Oslo: Stark Centimeter Wave Spectrometer*

The rotational spectrum was studied in the range 7–80 GHz using the Oslo Stark spectrometer which is described briefly in Møllendal et al. (2005, 2006). The accuracy of the spectral measurements is about 0.1 MHz for isolated lines but some lines are overlapped by much stronger ground-state lines and are given an uncertainty of 0.2 MHz. The measurement of the dipole moment was performed using the Stark spectrometer in Oslo. Details of the construction and operation of this device, which has a 2 m Hewlett–Packard Stark cell, have been described elsewhere (Møllendal et al. 2005, 2006).

### *2.3. Lille: Submillimeter-wave Spectrometer*

The submillimeter-wave measurements (580–661 GHz) were performed in Lille with a source-modulated spectrometer using phase-stabilized backward wave oscillators (BWO) working in

the frequency range 150–670 GHz. More details could be found in Willaert et al. (2006). The absorption was detected with a liquid helium cooled InSb bolometer (QMC Instruments Ltd). The measurements were made at room temperature and the pressure in the absorption cell was from 10 to 30 mTorr. The line width of the lines is Doppler limited. The accuracy of the measurements is about 30 kHz for isolated lines. However, if the lines are blended or with a poor signal-to-noise ratio, they were given a weight of 100 or even 200 kHz.

### 2.4. Sample

The sample is commercial; it was purchased from Aldrich and was used without further purification.

## 3. THEORETICAL MODEL

The Hamiltonian used in the present work is the so-called RAM internal rotation Hamiltonian based on the work of Kirtman (1962), Lees & Baker (1968), Herbst et al. (1984). Since rather complete descriptions of this method, which takes its name from the choice of the axis system, have been presented in the literature (Lin & Swalen 1959; Hougen et al. 1994), we will not repeat here a detailed description. So far we have applied this formalism and our code to a number of internal rotor molecules (see, for example, Ilyushin et al. 2003), including methyl formate (Carvajal et al. 2007, 2009).

Like for the normal methyl formate species, the three-fold torsional potential barrier of $DCOOCH_3$ is rather high ($V_3 \approx 389\ cm^{-1}$) but the value of the reduced height $s = 4V_3/9F$ (with $F \approx 5.49\ cm^{-1}$ being the internal rotation constant) is about 31, so torsional splittings reach values up to a few MHz in the torsional ground state. In addition, like in the parent species of methyl formate, the presence of low-frequency small-amplitude vibrations in $DCOOCH_3$ (Shimanouchi 1972), the COC bending mode $\upsilon_{12}$ at 315 $cm^{-1}$, and the out-of-plane COC bending $\upsilon_{17}$ mode at 290 $cm^{-1}$, lying near the top of the barrier could cause some perturbations on the rotational–torsional energy levels under study but such perturbations were not observed during the course of the present work which includes only the ground torsional state.

As in the normal species of methyl formate, we observe a clustering of the transitions with the same $K_c$ quantum number for high $J$, low $K_a$ values. This clustering is the consequence of a relatively asymmetric near-prolate internal rotor molecule ($\kappa = -0.75$).

Finally, the labeling scheme for the methyl formate energy levels as well as the connection with the traditional $J_{K_a,K_c}$ labeling scheme is discussed in Carvajal et al. (2007) and references therein.

## 4. ASSIGNMENTS AND FIT

In the present paper, we present a combined analysis of (1) 816 and 10 lines with an 80 or 200 kHz uncertainty, respectively, out of the 885 lines originally measured by Oesterling et al. (1995), 5 lines from Curl (1959) weighted with 200 kHz; (2) 275 newly measured in Oslo with an uncertainty of 150–200 kHz, including remeasurements of 8 lines initially measured by Curl (1959); (3) 479 new unblended lines from Lille, measured using broadband recording in various frequency intervals between 580 and 661 GHz with an uncertainty of 50 kHz, and 79 blended lines from Lille weighted 100–200 kHz; and (4) 39 (14 of them actually involve remeasurements from lines initially published by Curl 1959) FTMW lines from Lille, with the quadrupole hyperfine structure of the D atom being analyzed in the principal axis system ($\chi_{aa} = -0.0232(15)$ MHz, $\chi_{bb} = 0.1072(18)$ MHz, and $\chi_{aa}+\chi_{bb}+\chi_{cc} = 0$), in order to fit the frequency of the calculated rotational transitions with uncertainties of 3 and 10 kHz for the E (unblended) and A (blended) components, respectively.

Starting from the same data set as in Oesterling et al. (1995) which includes 885 $\upsilon_t = 0$ microwave transitions, we refit the data using our program (Hougen et al. 1994; Ilyushin et al. 2003)[6] starting at low $J$ and going up progressively. During this process, and similarly to what was happening with the normal species, we noted that a number of previously published lines showed observed–calculated values which were much worse than the ones belonging to the rest of the same $K_a$ sub-branch. We have thus decided to take some of them out of the fit. In addition, based on our fitting residuals, we have allocated an increased weight of 200 kHz to 10 lines from Oesterling data, instead of the 100 kHz originally quoted by the authors (Oesterling et al. 1995). We note also that Maeda et al. (2008b) have made the same conclusion regarding some of the somewhat large discrepancies observed in their studies concerning the normal species which they attribute to previous FASSST measurements performed in 1999 since those measurements were made without averaging upward and downward scans in frequency.

As in $H^{12}COO^{12}CH_3$ (Ilyushin et al. 2009), we observed the same behavior for the close series of lines assigned to A and E components of the $R$ branch involving $K_a = 0$ and 1: at low $J$ values, the A components of those transitions are above the E components but this situation changes after $J = 39 \rightarrow 40$ (instead of $J = 38$ for the normal species) and the A component lines lie below the E components for $J$ values above 39.

The "best" fit allowed 24 parameters (less than the 31 parameters used in Oesterling et al. 1995) to be varied. The microwave rms deviations obtained are 94.2 kHz (for 1703 $\upsilon_t = 0$ lines), involving transitions with $J \leqslant 64$, $K_a \leqslant 36$ for the ground torsional state. The overall quality of the fit is illustrated in Table 1, which gives the rms deviations for transitions grouped according to their measurement uncertainties (weight in the fit was proportional to the reciprocal of squared uncertainty). The unitless standard deviation is 1.11, and each group of transitions almost fits to experimental uncertainties.

Table 2 presents the values for the rotation–torsion parameters used in our model, which includes up to sixth-order parameters, i.e., those with $n = l + m = 6$, where $n$ is the total order of the operator, $l$ is the order of the torsional part, and $m$ is the order of the rotational part, respectively, following the notation of our previous papers on the RAM (Hougen et al. 1994). In comparison with the previous work, only 24 parameters are needed to achieve nearly experimental accuracy. However, because no direct information on the torsional vibrational frequency $\upsilon_t = 1$–0 is included in the fit, the correlation between the torsional parameters $F$ and $V_3$ is rather strong, and we fixed the value of the constant $F$ to its value for $H^{12}COO^{12}CH_3$ from Carvajal et al. (2007). This correlation between $F$ and $V_3$ is likely to increase the estimated uncertainty on the fitted $V_3$ parameter. Also, the value of the potential parameter $V_6$ cannot be determined while the potential barrier $V_3$ is being fitted with only experimental $\upsilon_t = 0$ transition lines. For this reason, the

[6] The source code for the fit, an example of input data file, and a readme file are available at the Web site (http://www.ifpan.edu.pl/~kisiel/introt/introt.htm#belgi) managed by Dr. Zbigniew Kisiel. Extended versions of code made in order to fit transitions with higher $J$ and $K$ are also available from two of the authors (I.K. and M.C.).

**Table 1**
rms Deviations from the Global Fit[a] of Transitions Involving $v_t = 0$ Torsional Energy Levels of Deuterated Methyl Formate ($DCOOCH_3$)

| | |
|---|---|
| Number of parameters | 24 |
| Number of lines | 1703 |
| rms of the 1703 MW $v_t$=0–0 lines | 0.0942 MHz |
| rms of the 882 A symmetry lines | 0.0971 MHz |
| rms of the 821 E symmetry lines | 0.0909 MHz |

| Source[b] | Range[c] (GHz) | $J_{max}$, $K_{max}$[d] | Number of Lines[e] | Uncertainties[f] (MHz) | rms[g] (MHz) |
|---|---|---|---|---|---|
| FTMW–Lille | 4–18 | 7,4 | 18 | 0.003 | 0.0047 |
| | | | 21 | 0.010 | 0.0154 |
| BWO–Lille | 580–661 | 64,36 | 479 | 0.050 | 0.0655 |
| OEST | 91–377 | 30,25 | 816 | 0.080 | 0.0799 |
| BWO–Lille | 580–661 | 57,29 | 48 | 0.100 | 0.1190 |
| OSLO | 7–80 | 48,16 | 259 | 0.150 | |
| | | | 16 | 0.200 | |
| BWO–Lille | 580–661 | 57,35 | 31 | 0.200 | 0.1493 |
| CURL | 227–290 | 5, 1 | 5 | 0.200 | |
| OEST | 91–377 | 26, 6 | 10 | 0.200 | |

**Notes.**
[a] Parameter values are given in Table 2. The complete list of observed minus calculated residuals of $v_t = 0$ lines is given in the machine-readable form of Table 3 in the online journal.
[b] Sources of data: OEST (Oesterling et al. 1995); BWO–Lille, FTMW–Lille, and OSLO data come from present work. The FTMW–Lille and OSLO data include remeasurements of 22 out of 27 lines from CURL (Curl 1959).
[c] Spectral range of the measurements.
[d] Maximum $J$ and $K_a$ for each group of measurements.
[e] Number of MW lines in each uncertainty group.
[f] Uncertainty in MHz used in the fit.
[g] rms deviation in MHz for each group.

**Table 2**
Torsion–Rotation Parameters Needed for the Global Fit of Transitions Involving $v_t = 0$ Torsional Energy Levels of Deuterated Methyl Formate ($DCOOCH_3$)

| $nlm$[a] | Operator[b] | Parameter | $DCOOCH_3$[c] | $nlm$ | Operator | Parameter | $DCOOCH_3$[c] |
|---|---|---|---|---|---|---|---|
| 220 | $(1-\cos 3\gamma)/2$ | $V_3$ | 389.33454(605)[d] | 404 | $-P^4$ | $D_J$ | 0.100940(570) $10^{-6}$ |
| | $P_\gamma^2$ | F | 5.49037663[e] | | $-P^2P_a^2$ | $D_{JK}$ | −0.86569(730) $10^{-6}$ |
| 211 | $P_\gamma P_a$ | $\rho$ | 0.08131779(519) | | $-P_a^4$ | $D_K$ | 0.26783(136) $10^{-5}$ |
| 202 | $P_a^2$ | $A^{RAM}$ | 0.5480676(128) | | $-2P^2(P_b^2-P_c^2)$ | $\delta_J$ | 0.18296(284) $10^{-7}$ |
| | $P_b^2$ | $B^{RAM}$ | 0.29289567(924) | | $-\{P_a^2,(P_b^2-P_c^2)\}$ | $\delta_K$ | 0.12510(376) $10^{-6}$ |
| | $P_c^2$ | $C^{RAM}$ | 0.170820348(359) | | $P^2(P_aP_b+P_bP_a)$ | $D_{abJ}$ | −0.44518(259) $10^{-6}$ |
| | $(P_aP_b+P_bP_a)$ | $D_{ab}$ | −0.14593362(784) | | $(P_a^3P_b+P_bP_a^3)$ | $D_{abK}$ | 0.101139(207) $10^{-5}$ |
| 422 | $\sin 3\gamma(P_bP_c+P_cP_b)$ | $D_{bc}$ | 0.0007466(183) | 624 | $(1-\cos 3\gamma)(P_a^3P_b+P_bP_a^3)$ | $d_{abK}$ | −0.3648(162) $10^{-6}$ |
| | $(1-\cos 3\gamma)P^2$ | $F_v$ | −0.00234066(420) | 606 | $P^6$ | $H_J$ | −0.18(1) $10^{-13}$ |
| | $(1-\cos 3\gamma)P_a^2$ | $k_5$ | 0.0110040(378) | | $P^4P_a^2$ | $H_{JK}$ | 0.2663(29) $10^{-11}$ |
| | $(1-\cos 3\gamma)(P_b^2-P_c^2)$ | $c_2$ | −0.9645(416) $10^{-4}$ | | $\{P_a^4,(P_b^2-P_c^2)\}$ | $h_K$ | 0.4800(69) $10^{-11}$ |
| | $(1-\cos 3\gamma)(P_aP_b+P_bP_a)$ | $d_{ab}$ | −0.0057248(150) | | $P^2(P_a^3P_b+P_bP_a^3)$ | $D_{abJK}$ | −0.2382(52) $10^{-11}$ |
| 413 | $P_\gamma\{P_a,(P_b^2-P_c^2)\}$ | $c_4$ | 0.8508(292) $10^{-6}$ | | | | |

**Notes.**
[a] Notation from Ilyushin et al. (2003); $n = l + m$, where $n$ is the total order of the operator, $l$ is the order of the torsional part, and $m$ is the order of the rotational part.
[b] Notation from Ilyushin et al. (2003). $\{A, B\} = AB + BA$. The product of the parameter and operator from a given row yields the term actually used in the vibration–rotation–torsion Hamiltonian, except for $F$, $\rho$, and $A^{RAM}$, which occur in the Hamiltonian in the form $F(P_\gamma - \rho P_a)^2 + A^{RAM}P_a^2$.
[c] Values of the parameters from the present fit for the ground torsional state $v_t = 0$ of $DCOOCH_3$. All values are in $cm^{-1}$, except for $\rho$ which is unitless. Statistical uncertainties are given in parentheses in units of the last quoted digit.
[d] Effective value; see the text.
[e] Value of the internal rotation constant $F$ was kept fixed to the $HCOOCH_3$ value from Carvajal et al. (2007).

value of $V_6$ was kept fixed to zero and the value of $V_3$ determined in our fit can only be considered as an effective value, containing the contribution of $V_6$ (Carvajal et al. 2009).

Table 3 contains the highest frequency fitted lines; these are only part of the entire table with the line assignments available in the online edition: the observed frequencies with the measurement uncertainties (in parentheses), the calculated frequencies with the calculated uncertainties (in parentheses), the observed–calculated values, the line strengths for the transitions in the $v_t = 0$ torsional state, the lower state energies (referred to $J = K_a = 0$, A species taken as the zero of energy), and the references of the data sources.

When comparing different methods with each other, it is often useful to transform the RAM rotational constants into the PAM values. In Table 4, the RAM rotational constants obtained in the fitting (see Table 2) in MHz and their transformed values in the principal axis system PAM are presented. The 3 × 3 matrix of RAM rotational constants ($A^{RAM}$, $B^{RAM}$, $C^{RAM}$, plus the

**Table 3**
Results of the Global Fit of Ground Torsional State of Deuterated Methyl Formate ($DCOOCH_3$)

| Line Num.[a] | $vt'$ | $J'$ | $K'_a$ | $K'_c P'$ | $vt''$ | $J''$ | $K''_a$ | $K''_c P''$ | Obs. Freq.(Unc)[c] (MHz) | Calc. Freq. (Calc.Unc)[d] (MHz) | Obs–Calc[e] (MHz) | Line Str.[f] (D**2) | Lower Energy[g] ($cm^{-1}$) | |
|---|---|---|---|---|---|---|---|---|---|---|---|---|---|---|
| | Upper State[b] | | | | Lower State[b] | | | | | | | | | |
| 93158 | 0 | 55 | −26 | 30 | 0 | 54 | −26 | 29 | 658963.326(50) | 658963.172(21) | 0.154 | 115.108 | 873.5479 | BWO |
| 93029 | 0 | 55 | 26 | 29 | 0 | 54 | 26 | 28 | 658966.971(50) | 658966.878(20) | 0.093 | 115.111 | 873.5516 | BWO |
| 20108 | 0 | 55 | 24 | *(31+, 32-) | 0 | 54 | 24 | *(30+, 31−) | 659941.426(50) | 659941.373(18) | 0.053 | 240.186 | 832.3769 | BWO |
| 90633 | 0 | 55 | −24 | 32 | 0 | 54 | −24 | 31 | 659945.810(50) | 659945.723(19) | 0.087 | 120.091 | 832.3846 | BWO |
| 90498 | 0 | 55 | 24 | 31 | 0 | 54 | 24 | 30 | 659947.149(50) | 659947.002(21) | 0.147 | 120.095 | 832.3855 | BWO |
| 73044 | 0 | 52 | −12 | 40 | 0 | 51 | −12 | 39 | 660192.474(50) | 660192.574(27) | −0.100 | 133.979 | 599.6796 | BWO |
| 11048 | 0 | 52 | 12 | 40+ | 0 | 51 | 12 | 39+ | 660198.734(50) | 660198.687(27) | 0.047 | 133.973 | 599.6884 | BWO |
| 13528 | 0 | 54 | 15 | 40+ | 0 | 53 | 15 | 39+ | 660499.260(50) | 660499.184(18) | 0.076 | 134.736 | 669.5820 | BWO |
| 77672 | 0 | 54 | 15 | 40 | 0 | 53 | 15 | 39 | 660506.037(50) | 660506.114(20) | −0.077 | 134.375 | 669.5815 | BWO |
| 89327 | 0 | 55 | −23 | 33 | 0 | 54 | −23 | 32 | 660569.148(100) | 660569.162(21) | −0.014 | 122.440 | 813.0929 | BWO |

**Notes.**
[a] The first column is a line number, allowing to sort the lines by $J$ and $K$ sub-branches if needed.
[b] Upper and lower state quantum numbers are indicated by $'$ and $''$ respectively. Torsion–rotation levels of A species have a "parity" label; levels of E species have a signed $K_a$ value (Herbst et al. 1984). Note that for degenerate transitions, only the sum of line strengths of the degenerate transitions for a given cluster is preserved. Therefore, the degenerate clusters of transitions are represented by only one transition frequency accompanied by the sum of line strengths calculated for the cluster components. For those cases, instead of the usual label $J$, $K_a$, $K_c$, the cluster is represented by the rotational state designation $J$, * where the asterisk stands for the two degenerate levels with the same $J$, $K_c$ but with different $K_a$ quantum numbers, or with the same $J$, $K_a$ but with different $K_c$ quantum numbers. In the parentheses, for the A species, the two different $K_a$ (or $K_c$) levels and the parity quantum number "+" or "−" are indicated and means that those two levels are degenerate within the selected cutoff (0.005 MHz). For the E species, the parentheses contain + or $-K_a$ ($K_c$) and it means that those two levels are degenerate within the same selected cutoff (0.005 MHz).
[c] Observed $v_t = 0$ microwave transitions in MHz, with estimated uncertainties in parentheses (in kHz). Lines with 3 or 10 kHz measurement uncertainty are FTMW lines (4–18 GHz), the lines with 50, 100, or 200 kHz measurement uncertainty are Lille BWO lines (150–700 GHz), the lines with 150 and 200 kHz measurement uncertainty are OSLO lines (7–80 GHz), and the lines with a 80 or 200 kHz uncertainty come from Oesterling et al. (1995).
[d] Calculated line frequency in MHz with calculated uncertainty in kHz.
[e] Observed minus calculated values in MHz.
[f] Calculated line strengths in D**2 (for details of the calculation procedure, see the text).
[g] Lower state energy ($cm^{-1}$) referred to the $J = K_a = 0$ A-species energy level taken as the zero of the energy (zero-point torsional energy: 66.0929 $cm^{-1}$).
(This table is available in its entirety in a machine-readable form in the online journal. A portion is shown here for guidance regarding its form and content.)

off-diagonal inertia constant $D_{ab}$) was diagonalized using the values of those parameters from Table 2. This transformation corresponds to a rotation of the RAM axis system (where the $a$-axis lies along the direction of the $\rho$ vector) into the PAM axis system. This rotation is about the out-of-plane $c$-axis, which remains the same in the two axis systems. The angle $\theta_{\rm RAM}$ between the rho $a$-axis and the principal $a$-axis can be obtained from the following expression:

$$\tan(2\theta_{\rm RAM}) = \frac{2D_{ab}}{A - B}. \quad (1)$$

From the values of the rotational constants $A$, $B$, $C$, and $D_{ab}$ from Table 2, $\theta_{\rm RAM} = 24.^{\circ}42$. In Table 4, we also show the values of RAM and PAM constants for the normal species from Ilyushin et al. (2009).

## 5. INTENSITY CALCULATIONS

In the same way that the Hamiltonian was used in the calculation and fit of the line positions, the calculation of the line strengths was also carried out in the rho axis system. For this purpose, the components of the dipole moment must be expressed in this non-principal reference system. This approach and the equations used here are given in detail in Hougen et al. (1994), and it was also applied to the normal species (Carvajal et al. 2007) and to the $^{13}C$ species (Carvajal et al. 2009). Therefore, we do not repeat here the procedure to obtain the line strengths in the RAM system.

**Table 4**
Rotational Constants in the RAM and in the PAM for $DCOOCH_3$ and $H^{12}COO^{12}CH_3$

| Parameter | $DCOOCH_3$ | | $H^{12}COO^{12}CH_3$ | |
|---|---|---|---|---|
| | (RAM)[a] | (PAM)[b] | (RAM)[c] | (PAM)[d] |
| $A$(MHz) | 16430.65(38) | 18416.96(1.08) | 17629.39(21) | 19925.58(48) |
| $B$(MHz) | 8780.79(28) | 6794.48(24) | 9242.94(13) | 6946.75(23) |
| $C$(MHz) | 5121.065(11) | 5121.07(12) | 5318.021(78) | 5318.02(16) |
| $D_{ab}$(MHz) | −4374.98(24) | | −4952.718(39) | |
| $<(i,a)$ | | 50.903 | | 53.058 |
| $\theta_{\rm RAM}$ | | 24.42 | | 24.87 |

**Notes.** Angles between the principal axis and the methyl top axis.
[a] Rotational constants obtained in our work for the RAM axis system (see Table 2).
[b] Rotational constants of our work transformed to the principal axis system and angles $<(i,a)$ and $\theta_{\rm RAM}$ in degrees between (1) the principal $a$-axis and the methyl top axis, (2) and between the principal $a$-axis and the RAM $a$-axis, respectively.
[c] Rotational constants obtained in Ilyushin et al. (2009) with the RAM axis system for the normal species.
[d] Rotational constants from Ilyushin et al. (2009) transformed to the principal axis system and angles $<(i,a)$ and $\theta_{\rm RAM}$ in degrees between (1) the principal $a$-axis and the methyl top axis, (2) and between the principal $a$-axis and the RAM $a$-axis, respectively.

As in our previous studies on $H^{12}COO^{12}CH_3$ and the $^{13}C$ isotopologues, our intensity calculations are based on the assumption that the microwave intensities are only determined by the permanent electric dipole moments (Hougen et al.

**Table 5**
Second-order Stark Coefficients[a,b] and Dipole Moment[b,c] of $HCOOCH_3$

| Transition | | $\Delta\nu$ $E^{-2}/10^{-6}$ MHz $V^{-2}$ $cm^2$ | |
|---|---|---|---|
| | | Obs. | Calc. |
| $2_{1,2} \leftarrow 1_{1,1}$ | M = 0 | 6.75(7) | 7.00 |
| $2_{0,2} \leftarrow 1_{0,1}$ | M = 0 | −7.69(8) | −7.49 |
| | \|M\| = 1 | 9.29(11) | 9.29 |
| $2_{1,1} \leftarrow 1_{1,0}$ | M = 0 | 6.65(7) | 6.70 |
| $3_{1,3} \leftarrow 2_{1,2}$ | \|M\| = 1 | 3.80(6) | 3.70 |
| $3_{0,3} \leftarrow 2_{0,2}$ | M = 0 | −1.75(3) | −1.66 |
| | \|M\| = 2 | 4.35(6) | 4.44 |
| $3_{2,1} \leftarrow 2_{2,0}$ | M = 0 | 3.64(5) | 3.65 |
| $3_{1,2} \leftarrow 2_{1,1}$ | M = 0 | −10.1(2) | −9.94 |

**Notes.**
[a] A-symmetry species.
[b] Uncertainties represent one standard deviation.
[c] $\mu_a$ = 1.648(8), $\mu_b$ = 0.706(12), and $\mu_c$ = 0.0 (assumed), and $\mu_{tot}$ = 1.793(11) D (5.981(37) $10^{-30}$ C m); 1 D = 3.33564 $10^{-30}$ C m.

**Table 6**
Second-order Stark Coefficients[a,b] and Dipole Moment[b,c] of $DCOOCH_3$

| Transition | | $\Delta\nu$ $E^{-2}/10^{-6}$ MHz $V^{-2}$ $cm^2$ | |
|---|---|---|---|
| | | Obs. | Calc. |
| $2_{1,2} \leftarrow 1_{1,1}$ | M = 0 | 7.30(10) | 7.02 |
| $2_{0,2} \leftarrow 1_{0,1}$ | M = 0 | −7.85(10) | −7.56 |
| | \|M\| = 1 | 9.57(10) | 9.89 |
| $2_{1,1} \leftarrow 1_{1,0}$ | M = 0 | 7.64(8) | 7.39 |
| $3_{1,3} \leftarrow 2_{1,2}$ | \|M\| = 1 | 3.60(4) | 3.76 |
| $3_{0,3} \leftarrow 2_{0,2}$ | \|M\| = 2 | 4.77(5) | 4.88 |
| $3_{1,2} \leftarrow 2_{1,1}$ | \|M\| = 1 | −2.65(3) | −2.65 |
| $4_{1,4} \leftarrow 3_{1,3}$ | \| M \| = 1 | 6.14(6) | 6.00 |

**Notes.**
[a] A-symmetry species.
[b] Uncertainties represent one standard deviation.
[c] $\mu_a$ = 1.643(12), $\mu_b$ = 0.748(11), and $\mu_c$ = 0.0 (assumed), and $\mu_{tot}$ = 1.806(13) D (6.023(44) $10^{-30}$ C m); 1 D = 3.33564 $10^{-30}$ C m.

1994), without any dependence on the torsional angle and other vibrational coordinates.

## 6. DIPOLE MOMENT MEASUREMENTS

The dipole moments of $HCOOCH_3$ and $DCOOCH_3$ were determined in a least-squares fit using the experimental second-order Stark coefficients of the A-symmetry species transitions. The weight of each Stark coefficient was taken to be the inverse square of its standard deviation shown in Tables 5 and 6. The calculations of the theoretical values of the Stark coefficients were made using program MB04 (Marstokk & Møllendal 1969), which is based on the second-order perturbation theory of Golden & Wilson (1948), using the reported rotational constants of these two species (Curl 1959). The cell was calibrated using carbonyl sulfide (OCS), whose dipole moment was taken to be 0.71521(20) D (Muenter 1968). Methyl formate is known to have a symmetry plane (Curl 1959) and $\mu_c$ was therefore assumed to be zero. The dipole moments of the parent and deuterated species are very similar as expected. The dipole moment of $HCOOCH_3$ has previously been reported to be (no uncertainties quoted) $\mu_a$ = 1.63, $\mu_b$ = 0.68, and $\mu_{tot}$ = 1.77 D (Curl 1959), compared to the present values, which are 1.648(8), 0.706(12), and 1.793(11) D, respectively. In the case of deuterated methyl formate, the permanent electric dipole moment components have the values $\mu_a$ = 1.643(12), $\mu_b$ = 0.748(11), and $\mu_c$ = 0.0 (assumed) and $\mu_{tot}$ = 1.806(13) D in the principal axis system. The RAM dipole moment components obtained by Equation (2) of Carvajal et al. (2007) after rotation from the principal axis are $\mu_a$ = 1.805 and $\mu_b$ = 0.0019 D. The line strengths for all the assigned transitions included in the fit were obtained and are presented fully in the online edition of Table 3 for the torsional ground state. The degenerated transition lines were considered as one line with a resultant intensity which is the sum of intensities of the cluster transition lines (Carvajal et al. 2009). These lines should be useful for astrophysicists in the identification of new spectral lines in the interstellar space.

## 7. TENTATIVE DETECTION IN ORION: ASTRONOMICAL OBSERVATION

The observations were carried out using the IRAM 30 m radio telescope during 2004 September (3 mm and 1.3 mm), 2005 March (2 mm), and 2005 April (3 mm and 1.3 mm). We have covered the total spectral range allowed by the 30 m receivers. The four SiS receivers operating at 3, 2, and 1.3 mm were used simultaneously. Each receiver was tuned to a single sideband with image rejections within 20–27 dB (3 mm receivers), 12–16 dB (2 mm receivers), and 13 dB (1.3 mm receivers).

System temperatures were 100–350 K for the 3 mm receivers, 200–500 K for the 2 mm receivers, and 200–800 K for the 1.3 mm receivers, depending on the particular frequency, weather conditions, and source elevation. The intensity scale was calibrated using two absorbers at different temperatures and using the atmospheric transmission model (Cernicharo 1985; Pardo et al. 2001).

Pointing and focus were regularly checked on nearby quasars 0420−014 and 0528+134. The observations were made in the balanced wobbler-switching mode, with a wobbling frequency of 0.5 Hz and a beam throw in azimuth of ±240. The back ends used were two filter banks with 512 × 1 MHz channels and a correlator providing two 512 MHz bandwidths and 1.25 MHz resolution. We have performed a spectral line survey for which the central frequencies were chosen in a systematically way: from 80 GHz to 115.5 GHz by 500 MHz for the 3 mm domain; from 130.250 GHz to 176.750 GHz by 500 MHz for the 2 mm; from 197 to 241 by 500 MHz for the 1.3 mm (low frequency); and from 241.250 to 281.750 GHz by 500 MHz for the 1.3 domain (high frequency). We pointed toward the (survey) position $\alpha = 5^h35^m14\overset{s}{.}5$, $\delta = -5^\circ22'30\overset{''}{.}0$ (J2000.0) corresponding to IRc2. The detailed procedure used for the analysis of the line survey is described in Tercero et al. (2010).

## 8. ASTRONOMICAL MODELING

The lines of $DCOOCH_3$ are just at the detection limit of the Orion line survey, and it is difficult to find a sufficient number of lines to conclude beyond doubt that this isotopologue has indeed been detected. We have proceeded in two steps: (1) modeling the main isotopologue, $HCOOCH_3$, for which a large number of lines are detected. These lines cover a large energy range and trace all the cloud components of this object. The modeling is constrained by the lines of the two $^{13}C$ isotopologues detected by Carvajal et al. (2009); (2) from the parameters obtained from $HCOOCH_3$, $H^{13}COOCH_3$, and $HCOO^{13}CH_3$ we predict the spectrum of $DCOOCH_3$ for different column densities until the predictions match the observations. Due to the large number of line blends in the 80–280 GHz domain, only around 10 lines

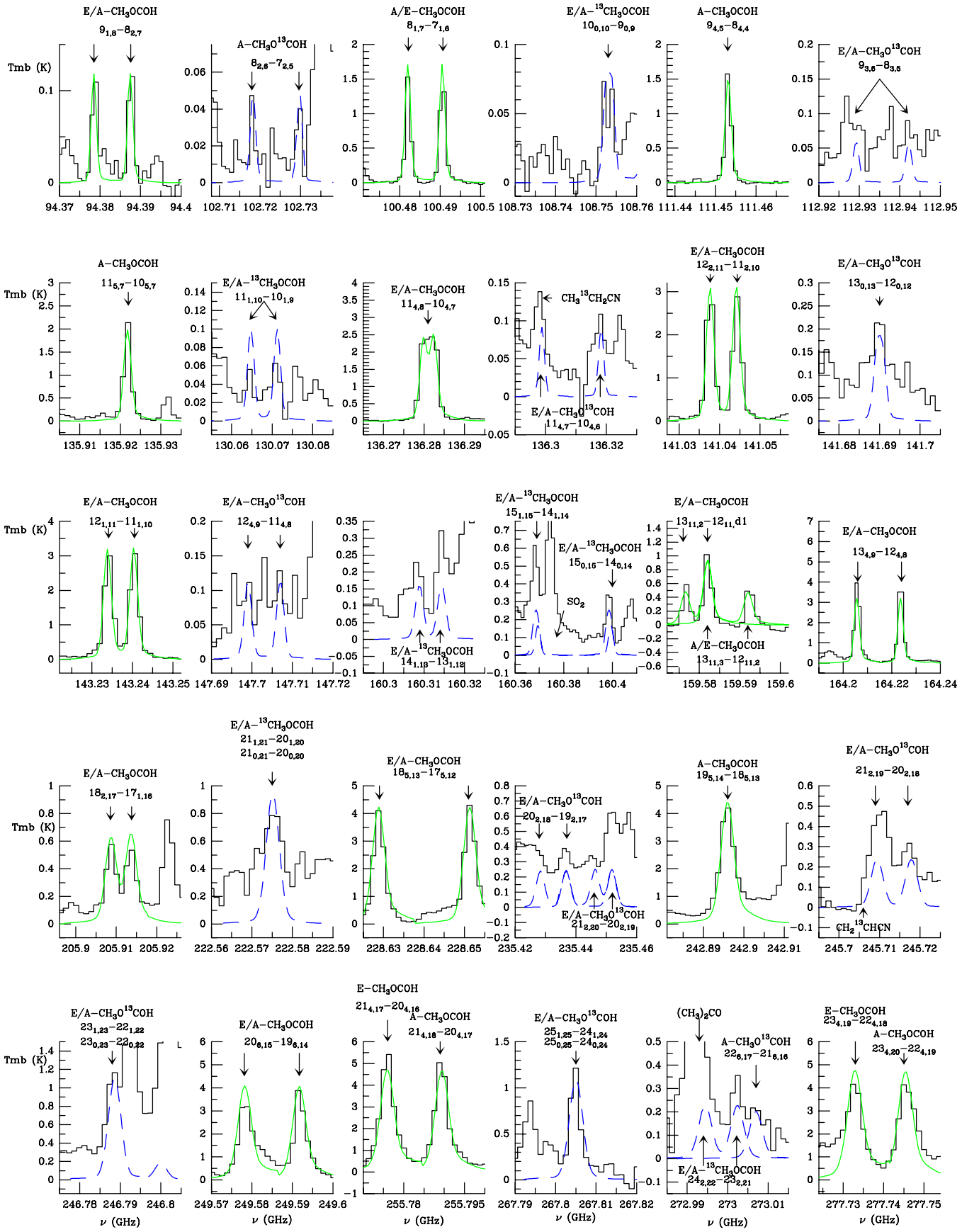


**Figure 3.** $HCOOCH_3$ and $^{13}C$ isotopologues selected lines detected in Orion. The histogram spectra are the observations compared to the model (smooth line for the main isotopologue and dashed line for the $^{13}C$ isotopologues).

(A color version of this figure is available in the online journal.)

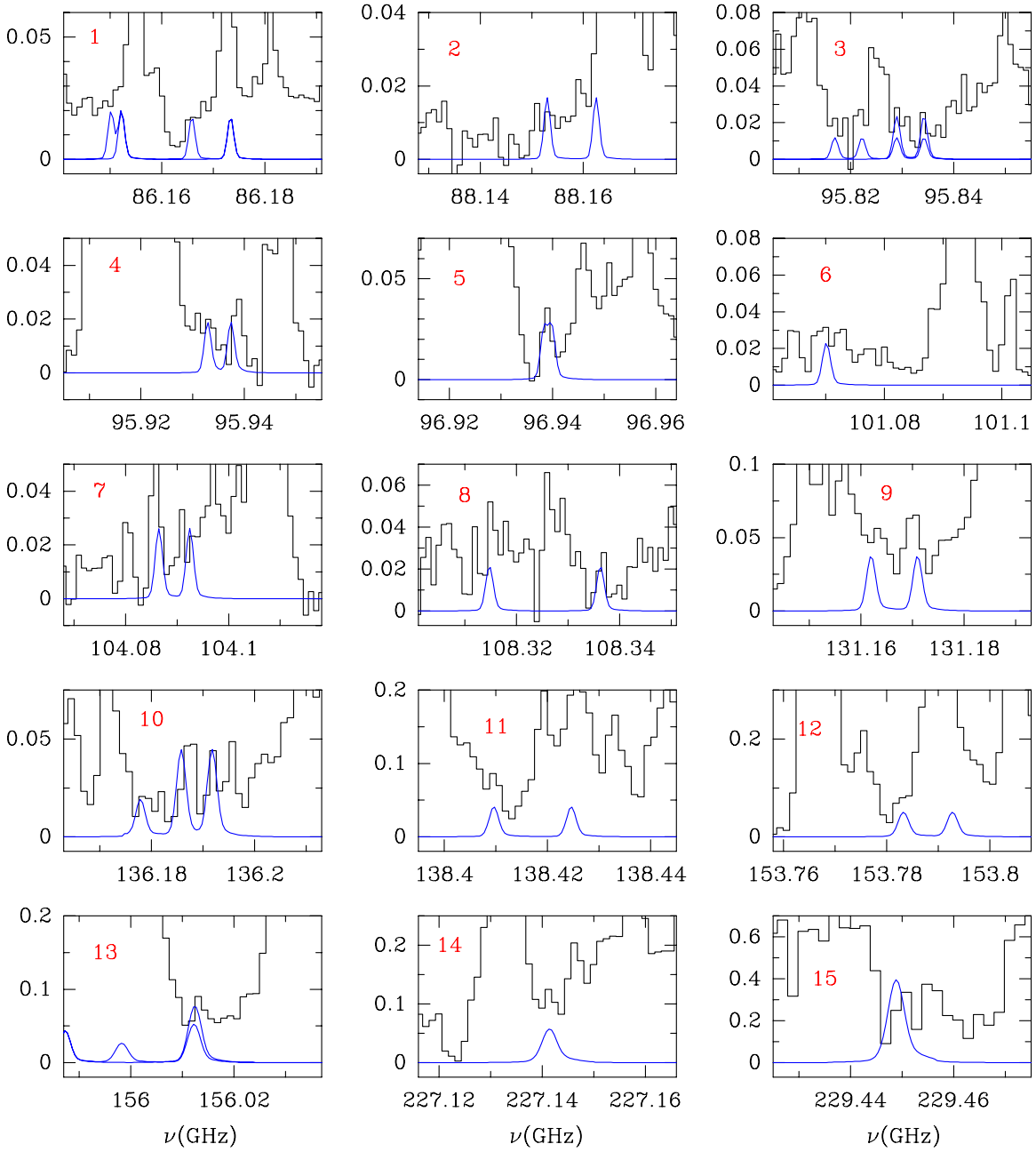


**Figure 4.** $DCOOCH_3$ detection in Orion. The spectra in all figures are in units of main beam temperature ($T_{mb}$, K). The histogram spectra are the observations compared to the model (smooth line). The data in panel 15 were observed in 2008 December with a spectral resolution of 2 MHz.

(A color version of this figure is available in the online journal.)

are clearly detected. However, more than 100 lines are partially blended and could be assigned to this isotopologue.

Four well-defined kinematic regions with quite different physical and chemical conditions (Blake et al. 1987, 1996) are implied by the observed LSR velocities and line widths in Orion KL: (1) the narrow ($\lesssim$5 km s$^{-1}$ line width) feature at $v_{LSR} \simeq$ 9 km s$^{-1}$ forming an N–S *extended ridge* or ambient cloud ($T_k \simeq$ 60 K); (2) a compact and quiescent region, *compact ridge*, ($v_{LSR} \simeq$ 7–8 km s$^{-1}$, $\Delta v \simeq$ 3 km s$^{-1}$) identified for the first time by Johansson et al. (1984; $T_k \simeq$ 110 K); (3) the more turbulent and compact *plateau* ($v_{LSR} \simeq$ 6–10 km s$^{-1}$, $\Delta v \gtrsim$ 25 km s$^{-1}$, $T_k \simeq$ 150 K); (4) the *hot core* component ($v_{LSR} \simeq$ 3–5 km s$^{-1}$, $\Delta v \lesssim$ 10–15 km s$^{-1}$, $T_k \simeq$ 225 K) first observed in ammonia emission (Morris et al. 1980). Methyl formate emission comes mainly from the compact ridge component as well as its isotolopogue emission (organic-saturated O-rich species detected in Orion seems to come mainly from this component).

From the detected lines of $HCOOCH_3$, we can separate the contribution of each component to the line emission. In order to reproduce the lines of the main isotopologue, we have added an additional component for the compact ridge with a kinetic temperature of 250 K. We have assumed LTE in all cases. The lack of collisional rates for this molecule avoids a more detailed analysis of the emission of methyl formate. Nevertheless, for most components it is known that this approximation works reasonably well. Only for the extended ridge could we have non-LTE conditions. However, the lines affected by this cloud

**Table 7**
Emission lines of $DCOOCH_3$ (Without High Blend) Present in the Frequency Range of the Orion KL Survey

| $J'$ | $K'_a$ | $K'_c$ | $P'$ | $J''$ | $K''_a$ | $K''_c$ | $P''$ | Predicted Frequency (MHz) | $S_{ij}$ ($D^2$) | $E_{\rm lower}$ ($cm^{-1}$) | Observed Frequency (MHz) | Observed $T_{\rm mb}$ (K) | Modeled $T_{\rm mb}$ (K) |
|---|---|---|---|---|---|---|---|---|---|---|---|---|---|
| 7 | 6 | 2 | E | 6 | 6 | 1 | E | 83611.554 | 5.017 | 23.3844 | 83612.1 | 0.008 | 0.006 |
| 7 | 6 | 2 | A | 6 | 6 | 1 | A | 83612.365 | 5.018 | 23.3826 | (a) | | |
| 7 | 6 | 1 | A | 6 | 6 | 0 | A | 83612.378 | 5.018 | 23.3826 | (a) | | |
| 7 | 4 | 4 | A | 6 | 4 | 3 | A | 83940.506 | 12.737 | 15.0476 | 83940.0 | 0.004 | 0.008 |
| 7 | 3 | 5 | A | 6 | 3 | 4 | A | 83953.879 | 15.425 | 12.1354 | 83954.1 | 0.020 | 0.016 |
| 7 | 3 | 5 | E | 6 | 3 | 4 | E | 83954.703 | 15.347 | 12.1466 | (a) | | |
| 7 | 4 | 4 | E | 6 | 4 | 3 | E | 83961.834 | 12.566 | 15.0543 | 83961.0 | 0.011 | 0.008 |
| 7 | 4 | 3 | E | 6 | 4 | 2 | E | 83968.959 | 12.568 | 15.0631 | 83970.1 | 0.014[b] | 0.008 |
| 7 | 4 | 3 | A | 6 | 4 | 2 | A | 84002.064 | 12.737 | 15.0484 | 84002.1 | 0.021[c] | 0.008 |
| 7 | 3 | 4 | E | 6 | 3 | 3 | E | 85113.227 | 15.353 | 12.1749 | 85114.1 | 0.017 | 0.008 |
| 7 | 3 | 4 | A | 6 | 3 | 3 | A | 85127.860 | 15.431 | 12.1629 | 85127.1 | 0.012 | 0.008 |
| 8 | 1 | 8 | E | 7 | 1 | 7 | E | 86150.519 | 21.130 | 10.6281 | 86150.9 | 0.031 | 0.020 |
| 8 | 1 | 8 | A | 7 | 1 | 7 | E | 86152.270 | 21.133 | 10.6150 | (a) | | |
| 7 | 1 | 6 | E | 6 | 1 | 5 | E | 86166.043 | 18.254 | 9.2357 | 86165.9 | 0.018 | 0.010 |
| 7 | 2 | 5 | E | 6 | 2 | 4 | E | 88152.955 | 17.418 | 10.2907 | 88153.1 | 0.009 | 0.009 |
| 8 | 6 | 3 | E | 7 | 6 | 2 | E | 95647.656 | 9.455 | 26.1734 | 95650.1 | 0.029[d] | 0.015 |
| 8 | 6 | 3 | A | 7 | 6 | 2 | A | 95648.608 | 9.456 | 26.1716 | (a) | | |
| 8 | 6 | 2 | A | 7 | 6 | 1 | A | 95648.691 | 9.456 | 26.1716 | (a) | | |
| 8 | 5 | 3 | E | 7 | 5 | 2 | E | 95822.442 | 13.169 | 21.6032 | 95822.0 | 0.033[b] | 0.008 |
| 8 | 5 | 4 | A | 7 | 5 | 3 | A | 95829.061 | 13.172 | 21.5886 | 95829.0 | 0.034 | 0.016 |
| 8 | 5 | 4 | E | 7 | 5 | 3 | E | 95829.291 | 13.169 | 21.5927 | (a) | | |
| 8 | 5 | 3 | A | 7 | 5 | 2 | A | 95834.355 | 13.172 | 21.5887 | 95834.1 | 0.032[b] | 0.008 |
| 8 | 3 | 6 | E | 7 | 3 | 5 | E | 95932.937 | 18.532 | 14.9470 | 95933.0 | 0.020 | 0.012 |
| 9 | 0 | 9 | E | 8 | 0 | 8 | E | 96938.275 | 23.863 | 13.4666 | 96939.0 | 0.042 | 0.032 |
| 9 | 0 | 9 | A | 8 | 0 | 8 | A | 96939.945 | 23.867 | 13.4536 | (a) | | |
| 8 | 1 | 7 | E | 7 | 1 | 6 | E | 97220.792 | 20.853 | 12.1099 | 97219.0 | 0.041[e] | 0.013 |
| 8 | 1 | 7 | A | 7 | 1 | 6 | A | 97228.138 | 20.856 | 12.0976 | 97230.0 | 0.031[f] | 0.013 |
| 8 | 3 | 5 | E | 7 | 3 | 4 | E | 98112.239 | 18.554 | 15.0140 | 98110.0 | 0.045[b] | 0.012 |
| 8 | 3 | 5 | A | 7 | 3 | 4 | A | 98124.049 | 18.569 | 15.0025 | 98126.0 | 0.030[b] | 0.012 |
| 8 | 2 | 6 | E | 7 | 2 | 5 | E | 101059.432 | 20.317 | 13.2311 | 101061.0[b] | 0.016 | 0.015 |
| 8 | 2 | 6 | A | 7 | 2 | 5 | A | 101070.237 | 20.320 | 13.2193 | 101070.0 | 0.039 | 0.015 |
| 9 | 2 | 8 | A | 8 | 2 | 7 | A | 104092.599 | 22.919 | 15.7892 | 104092.9 | 0.026 | 0.017 |
| 9 | 8 | 1 | A | 8 | 8 | 0 | A | 107474.026 | 10.206 | 41.0348 | 107475.0 | 0.025 | 0.008 |
| 9 | 8 | 2 | A | 8 | 8 | 1 | A | 107474.026 | 10.206 | 41.0348 | (a) | | |
| 9 | 8 | 2 | E | 8 | 8 | 1 | E | 107476.041 | 5.102 | 41.0319 | (a) | | |
| 9 | 3 | 7 | A | 8 | 3 | 6 | A | 107825.061 | 21.565 | 18.1359 | 107826.0 | 0.037[b] | 0.016 |
| 9 | 5 | 5 | A | 8 | 5 | 4 | A | 107976.488 | 16.811 | 24.7852 | 107975.9 | 0.048[b] | 0.012 |
| 9 | 4 | 6 | A | 8 | 4 | 5 | A | 108314.902 | 19.508 | 21.0534 | 108315.0 | 0.039 | 0.015 |
| 9 | 4 | 6 | E | 8 | 4 | 5 | E | 108336.584 | 18.654 | 21.0619 | 108337.0 | 0.026 | 0.015 |
| 9 | 4 | 5 | E | 8 | 4 | 4 | E | 108663.706 | 18.656 | 21.0737 | 108664.9 | 0.011 | 0.015 |
| 9 | 3 | 6 | E | 8 | 3 | 5 | E | 111419.459 | 21.620 | 18.2866 | 111418.9[b] | 0.029 | 0.018 |
| 9 | 2 | 7 | E | 8 | 2 | 6 | E | 113646.980 | 23.134 | 16.6021 | 113647.0 | 0.074[b] | 0.021 |
| 10 | 2 | 9 | E | 9 | 2 | 8 | E | 114933.607 | 25.675 | 19.2731 | 114934.9 | 0.063[b] | 0.022 |
| 11 | 3 | 9 | E | 10 | 3 | 8 | E | 131162.300 | 27.379 | 25.7319 | 131163.2 | 0.058[f] | 0.030 |
| 11 | 3 | 9 | A | 10 | 3 | 8 | A | 131171.151 | 27.383 | 25.7213 | 131170.6 | 0.067 | 0.030 |
| 11 | 9 | 2 | A | 10 | 9 | 1 | A | 131421.209 | 19.644 | 55.6912 | 131422.0 | 0.080[g] | 0.021 |
| 11 | 9 | 3 | A | 10 | 9 | 2 | A | 131421.209 | 19.644 | 55.6912 | (a) | | |
| 11 | 9 | 3 | E | 10 | 9 | 2 | E | 131425.371 | 9.822 | 55.6861 | (a) | | |
| 11 | 7 | 4 | E | 10 | 7 | 3 | E | 131705.721 | 17.682 | 42.3703 | 131705.8 | 0.070 | 0.031 |
| 11 | 7 | 5 | A | 10 | 7 | 4 | A | 131716.715 | 17.684 | 42.3582 | 131714.8 | 0.167[h] | 0.095 |
| 11 | 7 | 4 | A | 10 | 7 | 3 | A | 131716.819 | 17.684 | 42.3582 | (a) | | |
| 11 | 7 | 5 | E | 10 | 7 | 4 | E | 131717.055 | 17.682 | 42.3577 | (a) | | |
| 11 | 6 | 6 | A | 10 | 6 | 5 | A | 131997.199 | 20.878 | 36.9527 | 131997.8 | 0.112 | 0.042 |
| 11 | 6 | 6 | E | 10 | 6 | 5 | E | 131997.730 | 20.874 | 36.9543 | (a) | | |
| 11 | 5 | 7 | E | 10 | 5 | 6 | E | 132466.294 | 22.882 | 32.4004 | 132467.0 | 0.097[b] | 0.024 |
| 11 | 5 | 6 | A | 10 | 5 | 5 | A | 132550.518 | 23.578 | 32.3980 | 132549.9 | 0.090[b] | 0.024 |
| 12 | 2 | 11 | E | 11 | 2 | 10 | E | 136186.018 | 31.125 | 27.2974 | 136188.1 | 0.033 | 0.035 |
| 12 | 2 | 11 | A | 11 | 2 | 10 | A | 136191.909 | 31.130 | 27.2859 | 136191.9 | 0.030 | 0.035 |
| 11 | 2 | 9 | E | 10 | 2 | 8 | E | 137531.686 | 28.531 | 24.5902 | 137531.8 | 0.040 | 0.034 |
| 13 | 1 | 13 | E | 12 | 1 | 12 | E | 137533.221 | 34.644 | 28.4339 | 137533.8 | 0.036 | 0.080 |
| 13 | 1 | 13 | A | 12 | 1 | 12 | A | 137534.665 | 34.649 | 28.4210 | (a) | | |
| 11 | 2 | 9 | A | 10 | 2 | 8 | A | 137543.900 | 28.535 | 24.5795 | 137543.8 | 0.037 | 0.034 |
| 13 | 0 | 13 | E | 12 | 0 | 12 | E | 137581.848 | 34.645 | 28.4303 | 137582.8 | 0.529[b] | 0.080 |
| 13 | 0 | 13 | A | 12 | 0 | 12 | A | 137583.261 | 34.651 | 28.4175 | (a) | | |
| 12 | 1 | 11 | E | 11 | 1 | 10 | E | 137801.709 | 31.225 | 27.1505 | 137800.7 | 0.064[i] | 0.036 |

**Table 7**
(Continued)

| $J'$ | $K'_a$ | $K'_c$ | $P'$ | $J''$ | $K''_a$ | $K''_c$ | $P''$ | Predicted Frequency (MHz) | $S_{ij}$ ($D^2$) | $E_{\rm lower}$ ($cm^{-1}$) | Observed Frequency (MHz) | Observed $T_{\rm mb}$ (K) | Modeled $T_{\rm mb}$ (K) |
|---|---|---|---|---|---|---|---|---|---|---|---|---|---|
| 11 | 3 | 8 | E | 10 | 3 | 7 | E | 138410.006 | 27.605 | 26.1700 | 138409.4 | 0.087 | 0.033 |
| 12 | 7 | 6 | A | 11 | 7 | 5 | A | 143843.908 | 21.388 | 46.7518 | 143843.8 | 0.100 | 0.062 |
| 12 | 7 | 6 | E | 11 | 7 | 5 | E | 143844.263 | 21.386 | 46.7513 | (a) | | |
| 12 | 7 | 5 | A | 11 | 7 | 4 | A | 143844.280 | 21.388 | 46.7518 | (a) | | |
| 12 | 5 | 7 | A | 11 | 5 | 6 | A | 144996.317 | 26.790 | 36.8194 | 144995.8 | 0.071 | 0.030 |
| 14 | 0 | 14 | E | 13 | 0 | 13 | E | 147782.593 | 37.345 | 33.0195 | 147785.7 | 0.134[b] | 0.094 |
| 14 | 0 | 14 | A | 13 | 0 | 13 | A | 147783.950 | 37.350 | 33.0067 | (a) | | |
| 12 | 2 | 10 | E | 11 | 2 | 9 | E | 148695.043 | 31.123 | 29.1778 | 148695.8 | 0.086 | 0.041 |
| 13 | 3 | 11 | E | 12 | 3 | 10 | E | 153783.372 | 32.996 | 34.8626 | 153782.7 | 0.088 | 0.043 |
| 13 | 8 | 6 | A | 12 | 8 | 5 | A | 155714.597 | 21.820 | 57.7837 | 155713.7 | 0.110 | 0.043 |
| 13 | 8 | 5 | A | 12 | 8 | 4 | A | 155714.624 | 21.820 | 57.7837 | (a) | | |
| 13 | 7 | 7 | A | 12 | 7 | 6 | A | 156011.734 | 24.939 | 51.5499 | 156013.1 | 0.109 | 0.067 |
| 13 | 7 | 7 | E | 12 | 7 | 6 | E | 156012.322 | 24.936 | 51.5494 | (a) | | |
| 13 | 7 | 6 | A | 12 | 7 | 5 | A | 156012.899 | 24.939 | 51.5500 | (a) | | |
| 13 | 4 | 10 | E | 12 | 4 | 9 | E | 156965.595 | 31.735 | 37.9577 | 156965.7 | 0.163[b] | 0.042 |
| 13 | 4 | 10 | A | 12 | 4 | 9 | A | 156975.973 | 31.742 | 37.9488 | 156975.7 | 0.177[b] | 0.042 |
| 13 | 5 | 9 | A | 12 | 5 | 8 | A | 157087.911 | 29.921 | 41.6413 | 157091.8 | 0.045 | 0.037 |
| 14 | 1 | 13 | E | 13 | 1 | 12 | E | 157693.540 | 36.558 | 36.6742 | 157692.7 | 0.130 | 0.050 |
| 14 | 1 | 13 | A | 13 | 1 | 12 | A | 157698.960 | 36.563 | 36.6632 | 157698.7 | 0.104 | 0.050 |
| 15 | 1 | 15 | E | 14 | 1 | 14 | E | 157973.663 | 40.044 | 37.9501 | 157973.7 | 0.449[j] | 0.108 |
| 15 | 1 | 15 | A | 14 | 1 | 14 | A | 157974.977 | 40.050 | 37.9373 | (a) | | |
| 15 | 0 | 15 | E | 14 | 0 | 14 | E | 157988.204 | 40.045 | 37.9490 | 157989.3 | 0.317[g] | 0.108 |
| 15 | 0 | 15 | A | 14 | 0 | 14 | A | 157989.504 | 40.050 | 37.9363 | (a) | | |
| 16 | 0 | 16 | E | 15 | 0 | 15 | E | 168196.330 | 42.745 | 43.2189 | 168195.5 | 0.105 | 0.120 |
| 16 | 0 | 16 | A | 15 | 0 | 15 | A | 168197.572 | 42.751 | 43.2062 | (a) | | |
| 14 | 7 | 8 | A | 13 | 7 | 7 | A | 168223.930 | 28.368 | 56.7539 | 168224.3 | 0.125 | 0.090 |
| 14 | 7 | 8 | E | 13 | 7 | 7 | E | 168225.350 | 28.365 | 56.7534 | (a) | | |
| 14 | 7 | 7 | A | 13 | 7 | 6 | E | 168227.211 | 28.368 | 56.7540 | (a) | | |
| 14 | 4 | 11 | E | 13 | 4 | 10 | E | 168900.753 | 34.643 | 43.1935 | 168900.6 | 0.116[b] | 0.048 |
| 18 | 2 | 17 | E | 17 | 2 | 16 | E | 198055.498 | 47.309 | 59.7387 | 198055.1 | 0.178[b] | 0.070 |
| 18 | 2 | 17 | A | 17 | 2 | 16 | A | 198060.815 | 47.315 | 59.7284 | 198058.9 | 0.199[k] | 0.070 |
| 17 | 2 | 15 | E | 16 | 2 | 14 | E | 198737.592 | 43.987 | 57.3899 | 198738.9[c] | 0.039 | 0.065 |
| 19 | 1 | 19 | E | 18 | 1 | 18 | E | 198823.210 | 50.850 | 61.0719 | 198827.6 | 0.597[b] | 0.210 |
| 19 | 1 | 19 | A | 18 | 1 | 18 | A | 198824.283 | 50.857 | 61.0594 | (a) | | |
| 19 | 0 | 19 | E | 18 | 0 | 18 | E | 198824.378 | 50.850 | 61.0719 | (a) | | |
| 19 | 0 | 19 | A | 18 | 0 | 18 | A | 198825.449 | 50.857 | 61.0593 | (a) | | |
| 17 | 14 | 3 | A | 16 | 14 | 2 | A | 203086.858 | 29.532 | 135.8809 | 203087.1 | 0.099[b] | 0.026 |
| 17 | 14 | 4 | A | 16 | 14 | 3 | A | 203086.858 | 29.532 | 135.8809 | (a) | | |
| 17 | 14 | 3 | E | 16 | 14 | 2 | E | 203087.642 | 14.766 | 135.8798 | (a) | | |
| 17 | 13 | 4 | E | 16 | 13 | 3 | E | 203181.182 | 19.056 | 124.6372 | 203184.6 | 0.114[b] | 0.037 |
| 17 | 13 | 4 | A | 16 | 13 | 3 | A | 203183.450 | 38.112 | 124.6362 | (a) | | |
| 17 | 13 | 5 | A | 16 | 13 | 4 | A | 203183.450 | 38.112 | 124.6362 | (a) | | |
| 17 | 4 | 14 | A | 16 | 4 | 13 | A | 203638.661 | 43.116 | 61.2594 | 203638.4 | 0.039 | 0.065 |
| 17 | 9 | 8 | E | 16 | 9 | 7 | E | 204013.519 | 33.048 | 88.0397 | 204010.8[b] | 0.056 | 0.035 |
| 17 | 9 | 9 | A | 16 | 9 | 8 | A | 204027.150 | 33.052 | 88.0323 | 204030.9 | 0.173[l] | 0.105 |
| 17 | 9 | 8 | A | 16 | 9 | 7 | A | 204027.223 | 33.052 | 88.0323 | (a) | | |
| 17 | 9 | 9 | E | 16 | 9 | 8 | E | 204032.203 | 33.051 | 88.0282 | (a) | | |
| 17 | 5 | 12 | A | 16 | 5 | 11 | A | 210694.442 | 41.981 | 65.2886 | 210695.1 | 0.171[b] | 0.065 |
| 18 | 15 | 3 | A | 17 | 15 | 2 | A | 215018.124 | 29.686 | 154.7308 | 215017.6 | 0.040[b] | 0.015 |
| 18 | 15 | 4 | A | 17 | 15 | 3 | A | 215018.124 | 29.686 | 154.7308 | (a) | | |
| 20 | 1 | 19 | E | 19 | 1 | 18 | E | 218507.660 | 52.701 | 73.2902 | 218511.3 | 0.363[f] | 0.150 |
| 20 | 1 | 19 | A | 19 | 1 | 18 | A | 218512.781 | 52.707 | 73.2802 | (a) | | |
| 19 | 13 | 6 | A | 18 | 13 | 5 | A | 227279.985 | 54.564 | 138.5928 | 227280.0 | 0.106[b] | 0.036 |
| 19 | 13 | 7 | A | 18 | 13 | 6 | A | 227279.985 | 54.564 | 138.5928 | (a) | | |
| 19 | 12 | 7 | A | 18 | 12 | 6 | A | 227461.590 | 61.680 | 128.1925 | 227460.0[b] | 0.179 | 0.047 |
| 19 | 12 | 8 | A | 18 | 12 | 7 | A | 227461.590 | 61.680 | 128.1925 | (a) | | |
| 19 | 11 | 8 | A | 18 | 11 | 7 | A | 227702.074 | 68.228 | 118.6323 | 227700.0[b] | 0.040 | 0.058 |
| 19 | 11 | 9 | A | 18 | 11 | 8 | A | 227702.074 | 68.228 | 118.6323 | (a) | | |
| 20 | 2 | 18 | A | 19 | 2 | 17 | A | 228447.643 | 51.988 | 78.2544 | 228446.2[b] | 0.122 | 0.075 |
| 21 | 2 | 20 | E | 20 | 2 | 19 | E | 228684.773 | 55.398 | 80.5800 | 228690.0 | 0.269[g] | 0.154 |
| 21 | 2 | 20 | A | 20 | 2 | 19 | A | 228689.870 | 55.404 | 80.5702 | (a) | | |
| 21 | 1 | 20 | E | 20 | 1 | 19 | E | 228700.450 | 55.398 | 80.5788 | 228703.7 | 0.250 | 0.156 |
| 21 | 1 | 20 | A | 20 | 1 | 19 | A | 228705.520 | 55.404 | 80.5690 | (a) | | |
| 19 | 8 | 11 | A | 18 | 8 | 10 | A | 229139.909 | 42.231 | 95.0459 | 229139.9 | 0.124 | 0.050 |
| 22 | 1 | 22 | E | 21 | 1 | 21 | E | 229448.227 | 58.960 | 81.9896 | 229448.7 | 0.495 | 0.320 |

**Table 7**
(Continued)

| $J'$ | $K'_a$ | $K'_c$ | $P'$ | $J''$ | $K''_a$ | $K''_c$ | $P''$ | Predicted Frequency (MHz) | $S_{ij}$ ($D^2$) | $E_{lower}$ ($cm^{-1}$) | Observed Frequency (MHz) | Observed $T_{mb}$ (K) | Modeled $T_{mb}$ (K) |
|---|---|---|---|---|---|---|---|---|---|---|---|---|---|
| 22 | 0 | 22 | E | 21 | 0 | 21 | E | 229448.393 | 58.960 | 81.9896 | (a) | | |
| 22 | 1 | 22 | A | 21 | 1 | 21 | A | 229449.129 | 58.967 | 81.9772 | (a) | | |
| 22 | 0 | 22 | A | 21 | 0 | 21 | A | 229449.295 | 58.967 | 81.9771 | (a) | | |
| 19 | 3 | 16 | E | 18 | 3 | 15 | E | 230904.073 | 48.987 | 74.6431 | 230905.1 | 0.189[b] | 0.075 |
| 19 | 3 | 16 | A | 18 | 3 | 15 | A | 230915.564 | 48.992 | 74.6370 | 230915.0 | 0.194 | 0.075 |
| 19 | 6 | 14 | E | 18 | 6 | 13 | E | 230982.729 | 46.166 | 83.6832 | 230981.2 | 0.104 | 0.062 |
| 19 | 6 | 13 | E | 18 | 6 | 12 | E | 232824.423 | 46.181 | 83.7599 | 232823.3 | 0.172 | 0.063 |
| 21 | 3 | 19 | E | 20 | 3 | 18 | E | 238184.362 | 54.655 | 85.9074 | 238184.3 | 0.230[b] | 0.075 |
| 23 | 1 | 23 | E | 22 | 1 | 22 | E | 239654.547 | 61.664 | 89.6432 | 239655.0 | 0.479 | 0.350 |
| 23 | 0 | 23 | E | 22 | 0 | 22 | E | 239654.633 | 61.664 | 89.6432 | (a) | | |
| 23 | 1 | 23 | A | 22 | 1 | 22 | A | 239655.394 | 61.671 | 89.6308 | (a) | | |
| 23 | 0 | 23 | A | 22 | 0 | 22 | A | 239655.479 | 61.671 | 89.6307 | (a) | | |
| 23 | 1 | 22 | E | 22 | 1 | 21 | E | 249093.609 | 60.796 | 96.1762 | 249092.6 | 0.868[b] | 0.184 |
| 23 | 2 | 22 | A | 22 | 2 | 21 | A | 249093.810 | 60.801 | 96.1671 | (a) | | |
| 21 | 3 | 18 | E | 20 | 3 | 17 | E | 249997.096 | 54.143 | 90.3663 | 249997.2 | 0.093 | 0.076 |
| 20 | 5 | 15 | E | 19 | 5 | 14 | E | 252725.465 | 50.895 | 87.7814 | 252724.2 | 0.195[b] | 0.075 |
| 21 | 6 | 16 | A | 20 | 6 | 15 | A | 255755.841 | 52.056 | 99.5035 | 255757.2 | 0.146[b] | 0.067 |
| 21 | 7 | 14 | E | 20 | 7 | 13 | E | 255766.912 | 50.141 | 104.7105 | 255767.2 | 0.198[b] | 0.061 |
| 23 | 3 | 21 | E | 22 | 3 | 20 | E | 258615.279 | 60.033 | 102.1383 | 258611.2 | 0.290[n] | 0.076 |
| 23 | 3 | 21 | A | 22 | 3 | 20 | A | 258623.487 | 60.038 | 102.1314 | 258622.2 | 0.266[o] | 0.076 |
| 22 | 14 | 8 | E | 21 | 14 | 7 | E | 263324.309 | 35.338 | 173.7652 | 263323.7 | 0.110 | 0.056 |
| 22 | 14 | 8 | A | 21 | 14 | 7 | A | 263324.918 | 70.678 | 173.7662 | (a) | | |
| 22 | 14 | 9 | A | 21 | 14 | 8 | A | 263324.918 | 70.678 | 173.7662 | (a) | | |
| 22 | 12 | 10 | A | 21 | 12 | 9 | A | 263837.233 | 83.470 | 152.1663 | 263837.2 | 0.259[b] | 0.058 |
| 22 | 12 | 11 | A | 21 | 12 | 10 | A | 263837.233 | 83.470 | 152.1663 | (a) | | |
| 22 | 12 | 11 | E | 21 | 12 | 10 | E | 263851.647 | 41.736 | 152.1593 | 263852.1 | 0.160[b] | 0.029 |
| 21 | 5 | 16 | A | 20 | 5 | 15 | A | 266340.485 | 53.824 | 96.2081 | 266338.8 | 0.089 | 0.076 |
| 25 | 2 | 24 | E | 24 | 2 | 23 | E | 269487.933 | 66.197 | 113.1342 | 269490.0 | 1.209[g] | 0.599 |
| 25 | 1 | 24 | E | 24 | 1 | 23 | E | 269489.349 | 66.197 | 113.1341 | (a) | | |
| 25 | 2 | 24 | A | 24 | 2 | 23 | A | 269492.808 | 66.202 | 113.1251 | (a) | | |
| 24 | 3 | 21 | E | 23 | 3 | 20 | E | 279191.643 | 62.087 | 116.3492 | 279191.3 | 0.271 | 0.073 |
| 24 | 3 | 21 | A | 23 | 3 | 20 | A | 279201.345 | 62.091 | 116.3448 | 279201.2 | 0.304 | 0.073 |
| 27 | 1 | 27 | E | 26 | 1 | 26 | E | 280468.607 | 72.488 | 123.6616 | 280466.3[g] | 0.441 | 0.310 |
| 27 | 0 | 27 | E | 26 | 0 | 26 | E | 280468.613 | 72.488 | 123.6616 | (a) | | |
| 27 | 1 | 27 | A | 26 | 1 | 26 | A | 280469.236 | 72.494 | 123.6492 | (a) | | |
| 27 | 0 | 27 | A | 26 | 0 | 26 | A | 280469.242 | 72.494 | 123.6492 | (a) | | |

**Notes.** Emission lines of $CH_3OCOD$ (without high blend) present in the frequency range of the Orion KL survey. Columns 1–8 indicate the transition, Column 9 gives the calculated frequencies, Column 10 the line strength, Column 11 the energy of the lower level, Column 12 the observed (centroid) rest frequencies assuming that the radial velocities relative to LSR are 7.5 km $s^{-1}$, Column 13 the observed temperature of the main beam (at the peak of the line), and Column 14 the main beam temperature obtained with the model.

[a] Blended with the last one.
[b] Blended with the unidentified line.
[c] Blended with $CH_3OCOH$.
[d] Blended with t-$CH_3CH_2OH$.
[e] Blended with $^{13}CH_3OH$.
[f] Blended with $CH_3CH_2{}^{13}CN$.
[g] Blended with $(CH_3)_2CO$.
[h] Blended with $CH_3CH_2CN$ b type.
[i] Blended with $CH_2CH^{13}CN$.
[j] Blended with $CH_3CHO$.
[k] Blended with $O^{34}S^{18}O$.
[l] Blended with $H^{13}CCCN$ $\nu_7$=2.
[m] Blended with $HC_3N$ vibrationally excited.
[n] Blended with $CH_3{}^{13}CH_2CN$.
[o] Blended with $^{13}CH_3CH_2CN$.

component are those involving low energy levels for which its contribution is less than 50%. Its effect on the lines associated with high energy levels is negligible. Figure 3 shows the observations and the model for $HCOOCH_3$ and for the $^{13}C$ isotopologues. For the compact ridge, we assumed a source size of 15″ of diameter with uniform brightness temperature and optical depth over this size, placed 7″ from the pointed position. For the hot core component, we assumed a source size of 10″ placed 2″ from IRc2. The column densities calculated for the main isotopologue are $7 \times 10^{15}$, $5 \times 10^{15}$, $5 \times 10^{15}$, $2 \times 10^{15}$, and $1.5 \times 10^{15}$ $cm^{-2}$ for the "hot" compact ridge, compact ridge, hot core, extended ridge, and plateau, respectively, obtaining a

total column density of $2 \times 10^{16}$ cm$^{-2}$ (in agreement with the discussion in our previous paper, Carvajal et al. 2009).

From these models, i.e., fixing the temperatures and source structure, we have computed the $DCOOCH_3$ (A, E) lines for different column densities. The column densities obtained for reproducing the bulk of the $DCOOCH_3$ emission are $4 \times 10^{14}$, $1 \times 10^{14}$, $2 \times 10^{14}$, $5 \times 10^{13}$, and $3 \times 10^{13}$ cm$^{-2}$ for the "hot" compact ridge, compact ridge, hot core, extended ridge, and plateau, respectively. The model parameters were fixed to those derived from the analysis of the main isotope and other species (see Tercero et al., 2010). The fit has been made by a close inspection of the data and the model but not by minimizing through least-squares methods. Only the column density and the temperature of the gas were allowed to vary for the main isotope. When we considered that the fit was all right within 30%, then we fixed the parameters and allowed them to vary the column density for the deuterated species. A complete analysis will require to fit all lines (16,000 thousand lines of the survey) in order to have a correct minimization of the data. Hence, we proceeded by minimizing the intensity residuals until agreement was reached within 30% again. The uncertainty in the results is within a factor of 1.3–1.5.

Our results indicate a $DCOOCH_3/HCOOCH_3$ abundance ratio of 0.04 in the hot core, 0.06 in the "hot" compact ridge, 0.02 in the compact ridge, 0.025 in the extended ridge, and 0.02 in the plateau (similar ratios have been found by different authors in the compact ridge component; see Persson et al. 2007; Schilke et al. 1992; Tercero et al. 2010).

Table 7 gives the model predictions, observed peak intensities and frequencies, and predicted frequencies from the rotational constants obtained in this paper, for all lines of this isotopologue that are not strongly blended with other lines. $DCOOCH_3$ observed lines appear with a different degree of overlapping depending on the frequency domain: at 1.3 mm these lines are heavily blended, at 2 mm $DCOOCH_3$ lines are clearly detected, but blending is still important, while at 3 mm the lines are detected but they are very weak. The differences between the intensity of the model and the peak intensity of the observed lines are mostly due to the contribution from many other molecular species (the frequent overlap with other lines makes difficult to provide a good baseline for the weak lines of $DCOOCH_3$, especially at 1.3 mm). Figure 4 shows selected observed lines of $DCOOCH_3$ together with the model results (in units of $T_m b$). In spite of the amount of lines blended with other molecules, some panels of Figure 4 show a quite good agreement between the model and observations (see panels 2, 3, 5, 10,13, 15). Nevertheless, in all panels we assess the presence of $DCOOCH_3$ in the Orion KL spectra. It is worth noting that in $DCOOCH_3$, the two $^{13}$C isotopologues of methyl formate and four isotopologues of ethyl cyanide ($^{13}$C and $^{15}$N isotopologues; see Demyk et al. 2007; Margulès et al. 2009b; and Carvajal et al. 2009) contribute with more than 1600 lines in the 80–280 GHz domain covered by the Orion line survey of Tercero et al. (2010).

## 9. CONCLUSION

In this work, using the RAM, 24 rotation–torsion parameters of deuterated methyl formate, $DCOOCH_3$, have been obtained from a fit of 1703 lines (including some previously published 861 microwave lines and 842 new measurements) of the ground state $v_t = 0$ of this compound with a standard deviation of 94.2 kHz. The permanent dipole moment was measured for both the normal methyl formate and for $DCOOCH_3$ in order to improve the intensity calculation. In addition, the quadrupole hyperfine structure of the D atom was analyzed. A prediction of the line positions and intensities was produced to search for all the lines expected in the line survey of Orion and found 102 lines without heavy blending. In spite that these lines are at the detection limit of our survey (line confusion), most of these lines have a clear counterpart that can be related to deuterated methyl formate. None of the searched lines was missing (although around 300 are completely blended with other features) and many of them cannot be assigned to any other species. Hence, we claim a more than reasonable tentative detection of this species with a total column density of $\simeq 8\ 10^{14}$ cm$^{-2}$. Deuteration enhancement varies from 0.02 to 0.06 for the different cloud components of Orion.

It is now important to pursue the studies on the methyl formate isotopologues ($^{13}$C and deuterated species) by completing the measurements, analysis, and predictions for the first and second excited torsional states, as was recently done by Ilyushin et al. (2009) for the normal species. Indeed, without the excited torsional data, structural parameters such as the torsional barrier height and the internal rotation constant (as well as higher order terms in the potential Fourier series describing the potential internal rotation barrier) show high correlation, and their values can only be considered as effective values. Moreover, the knowledge of excited torsional states is also important for a future possible detection in the interstellar medium as shown by the detection of numerous lines for the first excited torsional $v_t = 1$ state of the $H^{12}COO^{12}CH_3$ species (Kobayashi et al. 2007; Demyk et al. 2008). In the case of the normal species, some of the second torsional excited state $v_t = 2$ transitions have turned out to be most likely perturbed by one of the other low-frequency small amplitude modes lying around, and the next step is thus to take into account those vibration–rotation–torsion interactions.

M.C. acknowledges the financial support provided by the Andalusian Government (Spain) project number P07-FQM-03014. He also thanks Université Paris 12 for inviting him. J.C., B.T., and N.M. thank the Spanish MICINN for support under grants AYA2006-14786, AYA2009-07304, and the CONSOLIDER program "ASTROMOL" CSD2009-00038. This work was supported by the program "National Physique et Chimie du Milieu Interstellaire." This work was also done under the ANR-08-BLAN-0054 and ANR-08-BLAN-0225. The authors also thank Dr. J. T. Hougen for numerous discussions during the work, Dr. V. V. Ilyushin for providing us various codes dealing with adding intensities of degenerate components, and providing information about the assignments and constants from his work on the normal species prior to publication. I.K. and J.D. thank the PEPCO-NEI cooperation project (MENESR, France)

## REFERENCES

Blake, G. A., Mundy, L. G., Carlstrom, J. E., Padin, S., Scott, S. L., Scoville, N. Z., & Woody, D. P. 1996, ApJ., 472, L49
Blake, G. A., Sutton, E. C., Masson, G. R., & Philips, T. G. 1986, ApJS, 60, 357
Blake, G. A., Sutton, E. C., Masson, C. R., & Philips, T. H. 1987, ApJ., 315, 621
Carvajal, M., Willaert, F., Demaison, J., & Kleiner, I. 2007, J. Mol. Spectrosc., 246, 158
Carvajal, M., et al. 2009, A&A, 500, 1109
Cernicharo, J. 1985, Internal IRAM Report (Granada: IRAM)
Curl, R. F. 1959, J. Chem. Phys., 30, 1529
Demyk, K., Wlodarczak, G., & Carvajal, M. 2008, A&A, 489, 589

Demyk, K., et al. 2007, A&A, 466, 255
Golden, S., & Wilson, E. B., Jr. 1948, J. Chem. Phys., 16, 669
Herbst, E. 1992, in Isotope Effects in gas Phase Chemistry, ed. J. A. Kaye (Washington, DC: Am. Chem. Soc.)
Herbst, E., Messer, J. K., De Lucia, F. C., & Helminger, P. 1984, J. Mol. Spectrosc., 108, 42
Hougen, J. T., Kleiner, I., & Godefroid, M. 1994, J. Mol. Spectrosc., 163, 559
Ilyushin, V., Alekseev, E. A., Dyubko, S. F., & Kleiner, I. 2003, J. Mol. Spectrosc., 220, 170
Ilyushin, V. V., Kryvda, A., & Alekseev, E. 2009, J. Mol. Spectrosc., 255, 32
Jacq, T., Walmsley, C. M., Mauersberger, R., Anderson, T., Herbst, E., & De Lucia, F. C. 1993, A&A, 272, 276
Johansson, L. E. B., et al. 1984, A&A, 130, 227
Kassi, S., Petitprez, D., & Wlodarczak, G. 2000, J. Mol. Struct., 517, 375
Kirtman, B. 1962, J. Chem. Phys., 37, 2516
Kobayashi, K., Ogata, K., Tsunekawa, S., & Takano, S. 2007, ApJ., 657, L17
Lees, R. M., & Baker, J. G. 1968, J. Chem. Phys., 48, 5299
Lin, C. C., & Swalen, J. D. 1959, Rev. Mod. Phys., 31, 841
Lovas, F. J. 2004, NIST Recommended Rest Frequencies for Observed Interstellar Molecular Microwave Transitions (Gaithersburg, MD: NIST), http://physics.nist.gov/cgi-bin/micro/table5/start.pl
Maeda, A., De Lucia, F. C., & Herbst, E. 2008a, J. Mol. Spectrosc., 251, 293
Maeda, A., Medvedev, I. R., De Lucia, F. C., & Herbst, E. 2008b, ApJS, 175, 138
Margulès, L., Coudert, L. H., Møllendal, H., Janekovà, R., Huet, T. R., & Guillemin, J. C. 2009a, J. Mol. Spectrosc., 254, 55
Margulès, L., et al. 2009b, A&A, 493, 565
Marstokk, K. M., & Møllendal, H. 1969, J. Mol. Struct., 4, 470
Mauersberger, R., Henkel, C., Jacq, T., & Walmsley, C. M. 1998, A&A, 194, L1
Møllendal, H., Cole, G. C., & Guillemin, J.-C. 2006, J. Phys. Chem. A, 110, 921
Møllendal, H., Leonov, A., & de Meijere, A. 2005, J. Phys. Chem. A, 109, 6344
Morris, M., Palmer, P., & Zuckerman, B. 1980, ApJ, 237, 1
Muenter, J. S. 1968, J. Chem. Phys., 48, 4544
Nummelin, A., Bergman, P., Hjalmarson, A., Friberg, P., Irwine, W. M., Millar, T. J., & Saito, S. 2000, ApJS., 128, 213
Oesterling, L. C., Ferguson, D. W., Herbst, E., & De Lucia, F. C. 1995, J. Mol. Spectrosc., 172, 469
Pardo, J. R., Cernicharo, J., & Serabyn, E. 2001, IEEE Trans. Antennas Propag., 49, 1683
Persson, C. M., et al. 2007, A&A, 476, 807
Schilke, P., Walmsley, C. M., Pineau Des Forets, G., Roueff, E., Flower, D. R., & Guilloteau, S. 1992, A&A, 256, 595
Shimanouchi, T. 1972, Tables of Molecular Vibrational Frequencies Consolidated Vol. 1 (Gaithersburg, MD: National Bureau of Standards), 1
Tercero, B., et al. 2010, A&A, in press
Willaert, F., Møllendal, H., Alekseev, E., Carvajal, M., Kleiner, I., & Demaison, J. 2006, J. Mol. Struct., 795, 4